Progress In Electromagnetics Research Letters, Vol. 97, 13–19, 2021

A Terahertz Demultiplexer Based on Metamaterials Applied to Terahertz Communication Systems

Wu Pan, Xuewen Zhang*, Yong Ma, Zhen Zhang, Xi Wang, Tao Shen, Yi Li, and Lihao Yang

Abstract—This paper proposes a novel terahertz demultiplexer based on metamaterials. Its surface metal structure comprises double U-shaped structures and a rectangular wire. The demultiplexer can separate terahertz of 0.225 THz and 0.410 THz, with high isolations of 41 dB and 38 dB, low insertion losses of 0.07 dB and 0.11 dB, and stable group delays of 3.5 ps and 3.8 ps at the center frequency, respectively. The equivalent parameters of metamaterials are simulated, and the electric field, current, and power distribution characteristics at operating frequency points are analyzed. This metamaterial is easy to process and is expected to be applied in future 6G wavelength division multiplexing systems.

1. INTRODUCTION

6G communication technology will become the focus of future communication systems due to its wider frequency band and faster transmission rate. As the frequency band is wider, the number of channels will be more, so the technology that can handle multiple channels efficiently is also required. In the field of optical communications, wavelength division multiplexing (WDM) technology that separates and integrates signals solves the problem of largecapacity transmission. In the terahertz band, we can also use WDM technology to multiplex and demultiplex terahertz waves. For WDM systems, in addition to the optical fiber for signal transmission, multiplexers and demultiplexers are vital components. However, because there is no complete communication protocol and system in the terahertz frequency band, a few researches on demultiplexers are applied to the terahertz frequency band.

In the microwave frequency band, a waveguide structure [1, 2] is the main structure of the wave demultiplexers or the power dividers, and good progress has been made. In the terahertz band, the current research on demultiplexers is mainly based on photonic crystal waveguides. Li et al. proposed a terahertz wavelength division multiplexer based on defect-coupled photonic crystal waveguides [3]. There are three transmission peaks in the frequency range of 1.07 to 1.16 THz, and the insertion losses are 1.92 dB, 0.96 dB, and 1.93 dB. The insertion loss of this demultiplexer is greater than 1 dB for both channels. Wu et al. proposed and designed a high-performance three-wavelength terahertz wavelength division multiplexer based on the graphene structure [4]. The center frequencies work at 8.2 THz, 8.6 THz, and 9.3 THz; the insertion losses are 0.81 dB, 0.04 dB, and 0.37 dB; isolation is about 15 dB; transmittance is greater than 50%. The insertion loss of this demultiplexer is small, but the isolation is not large enough. The other demultiplexers are summarized in Table 1. We can see that the insertion loss and isolation of the metamaterial demultiplexers are better. Because the terahertz wave has weak diffraction ability and is easily absorbed by rain, sand, and dust, it has a large attenuation in the natural environment. It is necessary to reduce the loss as much as possible in the 6G communication system, so the smaller the device's loss, the better. Otherwise, the photonic crystal is difficult to manufacture

Received 19 January 2021, Accepted 2 March 2021, Scheduled 15 March 2021

* Corresponding author: Xuewen Zhang (zxw0115@163.com).

The authors are with the Quantum Control and Quantum Device Technology Laboratory, College of Photoelectronic Engineering, University of Posts and Telecommunications, Chongqing 400065, China.

Table 1. Current work compared to other demultiplexers.

Refs.	Structure	Channels (THz)	Insertion Loss (dB)	Isolation (dB)
[5]	photonic crystal waveguides	0.323, 0.335	3	40, 15
[3]	photonic crystal waveguides	1.0385, 1.1125, 1.135	1.92, 0.96, 1.93	> 1
[6]	photonic crystal waveguides	0.325, 0.335	-	15
[7]	spoof surface plasmon polariton waveguides	0.637, 0.667	< 0.46	> 19
This work	Metamaterial	0.225, 0.410	0.07, 0.11	41, 38

and expensive, not conducive to large-scale production and promotion, which causes a high cost in the communication system.

This paper proposes a terahertz wave demultiplexer based on metamaterials used in terahertz communication windows. Metamaterials are artificial periodic materials [8], flexible, and adjustable, and have characteristics that natural materials do not have. For terahertz waves, we can modulate the phase [9], amplitude [10], and polarization state [11] of the terahertz wave by selecting a suitable metal pattern. Metamaterials' processing and production are easier than photonic crystals, conducive to large-scale promotion and use in the future. The demultiplexer proposed in this paper can separate terahertz waves with center frequencies of 0.225 THz and 0.410 THz. The isolations of the metamaterial at the center frequency are 41 dB and 38 dB, and the insertion losses are 0.07 dB and 0.11 dB. It has great application prospects in 6G wavelength division multiplexing systems. Firstly, we design a terahertz demultiplexer based on metamaterials. Secondly, we introduce metamaterials' theory and study the working mechanism of terahertz demultiplexers based on metamaterials. Finally, we summarize the main contents of this article.

2. METAMATERIAL AND DESIGN

When the metamaterial's periodicity length scale is smaller than the incident wavelengths of the electromagnetic band of operation, metamaterial can be regarded as a homogeneous material [12]. Like the material in nature, the homogeneous material has permittivity and permeability, which describe metamaterials' electromagnetic properties. Generally, ε_r is the effective permittivity and μ_r the effective permeability, which can be described by:

$$\varepsilon_r = \varepsilon' - i\varepsilon'' \tag{1}$$

$$\mu_r = \mu' - i\mu'' \tag{2}$$

According to the equivalent medium theory, the equivalent impedance of metamaterials can be expressed as [13]:

$$\frac{Z}{Z_0} = \sqrt{\frac{\mu_r}{\varepsilon_r}} \tag{3}$$

The effective impedance of the metamaterial can be obtained by S parameter, namely

$$Z = \sqrt{\frac{(1+S_{11})^2 - {S_{21}}^2}{(1-S_{11})^2 - {S_{21}}^2}} \tag{4}$$

By designing corresponding metal patterns, we can adjust the metamaterial's equivalent permittivity and permeability to change the metamaterial properties of the metamaterial [14].

3. SIMULATION AND RESULTS

Figure 1(a) shows the basic unit structure of the metamaterial. Figure 1(b) shows the array of the metamaterial. The surface metal pattern is gold, composed of a U-shaped metal ring and a rectangular

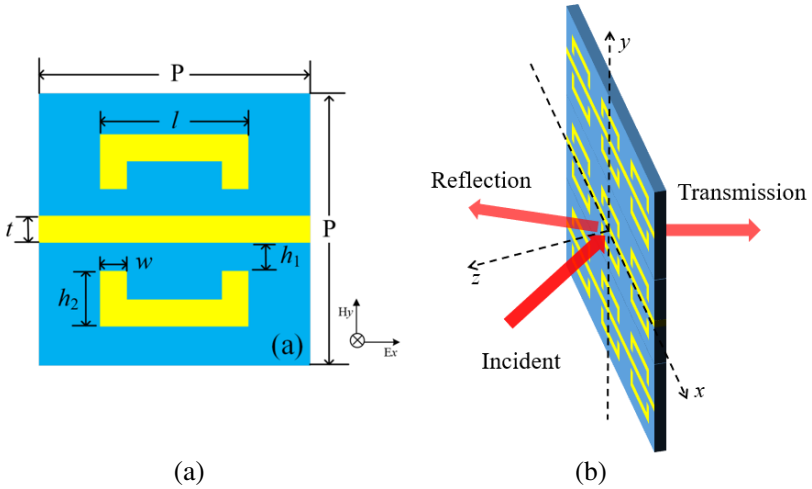

Figure 1. (a) Unit cell of metamaterial. The yellow part is metallic gold, and the blue part is polyimide. (b) The array of metamaterial. the terahertz wave is obliquely incident on the metamaterial surface from the xoz plane, and the angle with the z-axis is 10°.

metal wire. Since polyimide has high transmittance in the terahertz band, we select polyimide as the metamaterial substrate. The permittivity of polyimide is 3.4. Its dielectric loss angle is 0.0027. The cell size P is 420 μm, the U-shaped metal line length $l = 244$ μm, the line width $w = 50$ μm, the rectangular metal line width $t = 40$ μm, $h_1 = 40$ μm, $h_2 = 85$ μm. Simulating this structure in CST, setting the x and y directions as the unit cell boundary, the z-direction is the open boundary condition. For receiving convenience, the terahertz wave is incident on the metamaterial surface at an oblique angle of 10°.

Many methods have been proposed to obtain the effective parameters of metamaterials [15, 16]. By simulating the metamaterial in Computer Simulation Technology (CST), we can get the S parameters and then use the S parameters to retrieve the metamaterial's effective parameters. Figure 2(a) shows the normalized magnitude transmissivity and reflectivity of metamaterials. Both 0.225 THz and 0.410 THz are terahertz communication windows with the lowest points of transmissivity and reflectivity, respectively. The isolations at the two center frequency points are 41 dB and 38 dB, and the insertion losses are 0.07 dB and 0.11 dB.

Figure 2(b) shows the effective impedance curve of the metamaterial. At 0.225 THz, the real part of the effective impedance is close to 1 and the imaginary part close to 0, indicating that the metamaterial impedance matches the free space, so the reflected wave reaches the minimum. In the range of 0.300 THz $\sim$ 0.420 THz, the effective impedance of metamaterials is close to zero. Electromagnetic waves could stop or be stored when the real part of the impedance is near zero [17]. Figure 2(c) is the effective permittivity of the metamaterial, and Fig. 2(d) is the effective permeability of metamaterials. We can see that at 0.225 THz, the effective permittivity is $0.12-0.002j$, and the permeability is $0.11+0.001j$, so the effective impedance is close to 1. In the range of 0.23 THz $\sim$ 0.24 THz, the effective permittivity and permeability are close to zero, as shown in the shaded part, and some scholars have found that near-zero refractive index materials have the characteristics of high transmittance [18]. There are zero refractive indexes near 0.225 THz, which is the representation for the maximum transmittance of metamaterials. At 0.410 THz, the permittivity has a resonance peak, indicating that resonance has occurred at this frequency.

some scholars have found that near-zero refractive index materials have the characteristics of high transmittance.

There is an essential change in the 6G communication system, which has a higher transmission rate than 5G's 100 Gb/s, estimated to reach 1 Tb/s [19]. As the transmission rate increases, the group delay becomes smaller and smaller. The group delay is defined as:

$$d\tau = \frac{d\phi}{d\omega} \tag{5}$$

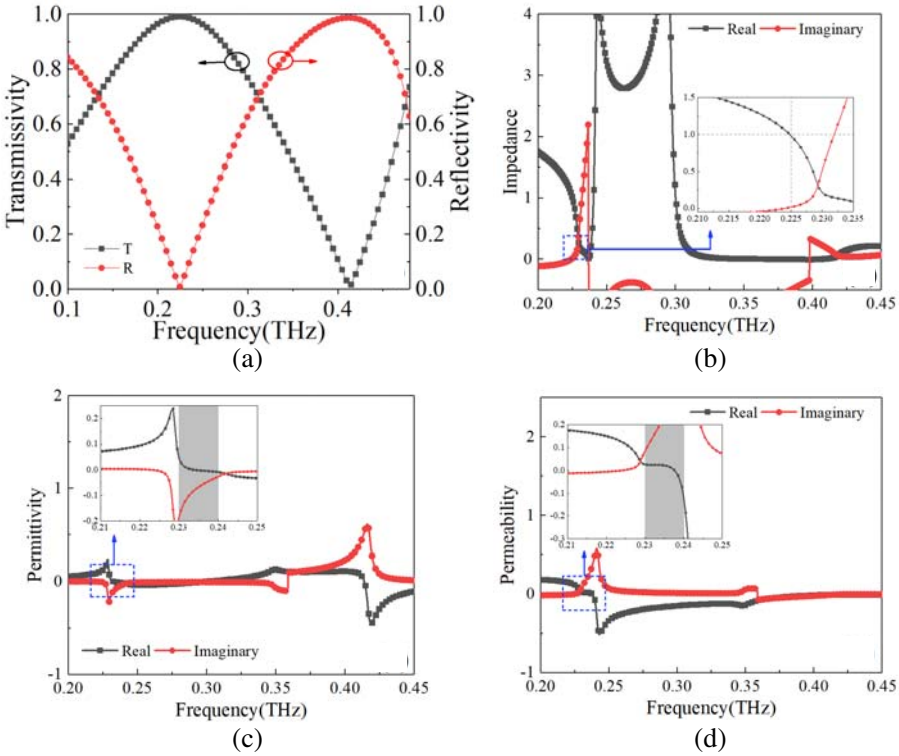

Figure 2. (a) Transmissivity and reflectivity of metamaterial. The black line is transmissivity and the red line is reflectivity (b) Effective impedance of metamaterial. The black line is the real part of the effective impedance, and the red line is the imaginary part of the effective impedance. (c) Effective permittivity of metamaterial. The black line is the real part of the effective permittivity, and the red line is the imaginary part of the effective permittivity. (d) Effective permeability of metamaterial. The black line is the real part of the effective permeability, and the red line is the imaginary part of the effective permeability.

In the above formula, ϕ represents the phase, and ω is the angular frequency. It is used for characterizing the distortion of information transmission. The more stable the group delay is, the less distortion the information will be. The group delay is obtained by calculating the phase of the metamaterial. Figures 3(a) and (b) show the group delay of metamaterials around 0.225 THz and 0.410 THz. The group delay at 0.225 THz is very stable and remains at around 3.5 ps. In the range of $0.200 \sim 0.300$ THz, the maximum group delay is 3.55 Ps; the minimum is 3.37 Ps; and the difference in group delay is 0.18 Ps. At 0.410 THz, the group delay of the metamaterial is stable at around 3.8 ps. In the range of $0.300 \sim 0.450$ THz, the maximum group delay is 4.22 Ps; the minimum is 3.39 Ps; and the difference in group delay is 0.83 Ps. We can see that the group delay near the two frequency points is very stable from the group delay's small difference. The group delay of metamaterials is in the Ps level, which can satisfy the low group delay requirements of future communication systems.

In order to further study the working mechanism of the metamaterial demultiplexer, we observe the electric field intensity, current density, and power distribution of the metamaterial at 0.225 THz and 0.410 THz. Figures 4(a) and (b) show the electric field distributions of metamaterials at 0.225 THz and 0.410 THz, respectively. At 0.225 THz, the electric field's energy is distributed in the area outside the metal, and there is no high-intensity electric field in the gap of the metal. At 0.410 THz, the electric field is mainly concentrated in the four regions adjacent to the double U-shaped structure and the rectangular line with no electric field around the metal pattern. The U-shaped structure and rectangular wire form an SRR with double gaps. This ring-shaped structure with gaps can form an LC mode [20] where inductance and capacitance exist. The direction of the ring electric field is normal to the gap of the capacitor. At this time, only the electric field can be coupled into the metamaterial [21]. According

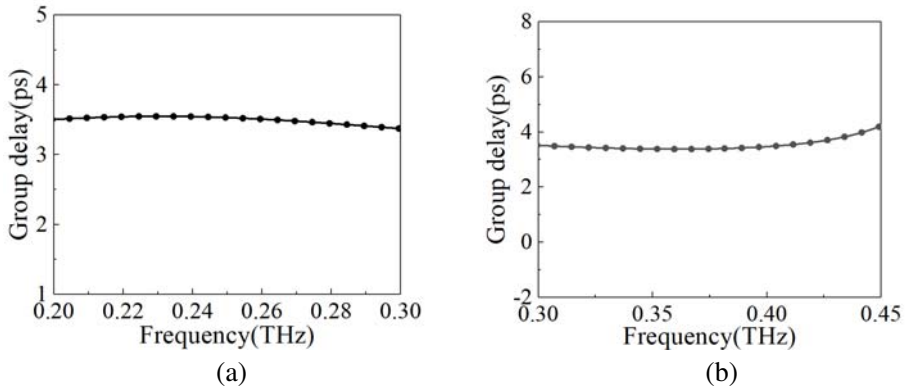

Figure 3. (a) Group delay at 0.225 THz and (b) Group delay at 0.410 THz.

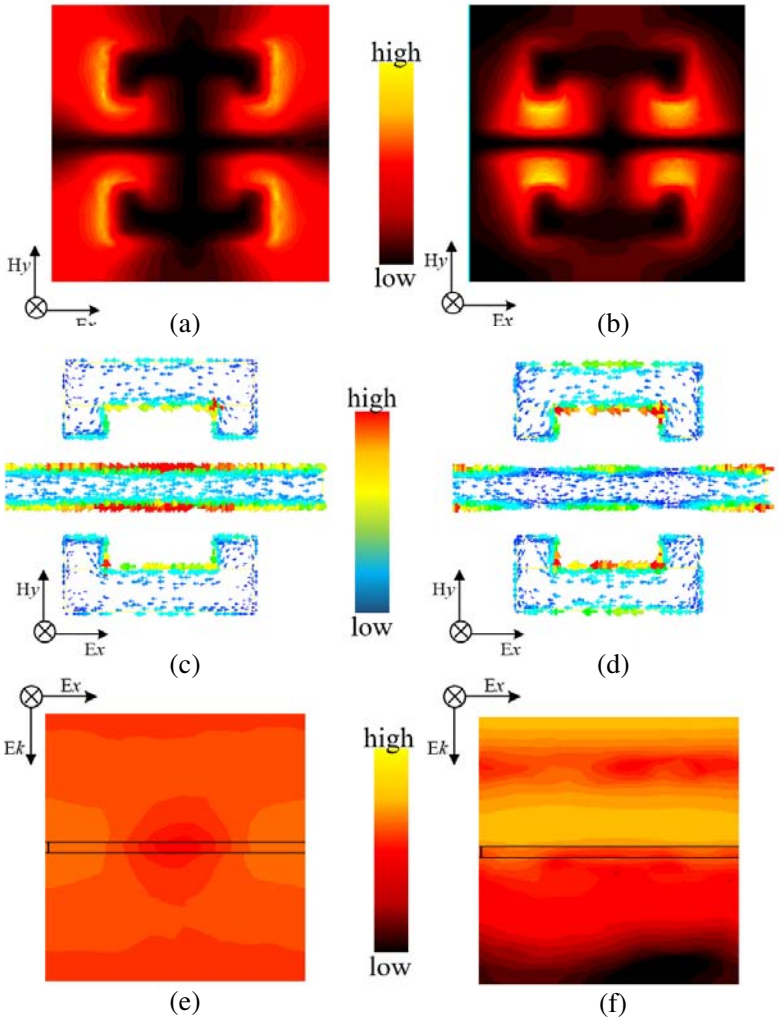

Figure 4. (a) Electric field distribution at 0.225 THz and (b) Electric field distribution at 0.410 THz. The electric field intensity in the yellow area is the largest, and the electric field intensity in the black area is the smallest. (c) Current distribution at 0.225 THz and (d) Current distribution at 0.410 THz. The red area has the highest current intensity and the blue area has the smallest current intensity. (e) Energy distribution at 0.225 THz and (f) Energy distribution at 0.410 THz. The black box in the middle is the cross-section of the metamaterial in xoz.

to Figure 2(c), there is an obvious electric resonance. Due to electrical resonance, it is difficult for the terahertz wave to pass through the metamaterial, and the metamaterial will reflect most of the terahertz wave. Therefore, the terahertz wave can be separated by the path. Figures 4(c) and (d) show the metamaterial's surface current distributions at 0.225 THz and 0.410 THz. It seems that the U-shaped structure and rectangular wire constitute a circular current, but the current on the rectangular wire at the gap does not appear suddenly reduced due to coupling. Therefore, no resonance occurs here, which is in good agreement with the above results. At 0.410 THz, due to the electric field's coupling, the current density at the gap is apparently reduced. It is worth mentioning that the current direction in the center of the rectangular line is opposite to that at the rest of the rectangular line. Since the terahertz wave is obliquely incident on the metamaterial surface, there will be a phase difference on the rectangular metal surface. The current flows from the high potential on the left to at the low potential on the right. As shown in Figure 4(b), the electric field intensity of the left gap is stronger than that of the right gap. Figures 4(e) and (f) are the energy distributions of the terahertz wave in xoz at 0.225 THz and 0.410 THz, respectively. At 0.225 THz, energy exists above and below the metamaterial, which means that the energy can pass through the metamaterial. At 0.410 THz, the energy is mainly distributed above the metamaterial, and there is also some energy below. There is no energy in the back, indicating that most terahertz waves do not pass through the metamaterial.

4. CONCLUSION

The demultiplexer based on metamaterials proposed in this paper can separate the 0.225 THz and 0.410 THz terahertz waves of the terahertz communication window with considerable isolation and small insertion loss in the working frequency band. The metamaterial achieves impedance matching at 0.225 THz, and resonance occurs at 0.410 THz to separate the two operating frequencies. Finally, we observe the metamaterial's electric field and surface current distribution. We find that in the 0.225 THz, there is no apparent resonance, but in the 0.410 THz, an electric resonance exists, which stops the transmission of the terahertz wave. This demultiplexer is expected to be applied to 6G wavelength division multiplexing systems due to its advantages, such as easy manufacture and flexible design.

ACKNOWLEDGMENT

This work was supported by New Direction Cultivation Project of Chongqing University of Posts and Telecommunications, China (A2014-116), the Key Research Program of Chongqing University of Posts and Telecommunications, China on Interdisciplinary and emerging field (A2018-01).

REFERENCES

1. Keshavarz, S., A. Abdipour, A. Mohammadi, et al., "Design and implementation of low loss and compact microstrip triplexer using CSRR loaded coupled lines," *International Journal of Electronics and Communications*, Vol. 111, 152913, 2019.
2. Keshavarz, S. and N. Nozhat, "Dual-band Wilkinson power divider based on composite right/left-handed transmission lines," *2016 13th International Conference on Electrical Engineering/Electronics, Computer, Telecommunications and Information Technology (ECTI-CON)*, 1–4, 2016.
3. Li, S., H. Liu, Q. Sun, et al., "Multi-channel terahertz wavelength division demultiplexer with defects-coupled photonic crystal waveguide," *Journal of Modern Optics*, Vol. 63, No. 10, 955–960, 2016.
4. Wu, X., Z. Lu, X. Guo, et al., "A graphene-based terahertz wavelength division multiplexer," *2015 IEEE International Symposium on Antennas and Propagation & USNC/URSI National Radio Science Meeting*, Vol. 63, No. 10, 1600–1601, 2015.
5. Yuan, M., Q. Wang, Y. Li, et al., "Ultra-compact terahertz plasmonic wavelength diplexer," *Applied Optics*, Vol. 59, No. 33, 10451–10456, 2020.

6. Withayachumnankul, W., M. Fujita, T. Nagatsuma, et al., "Integrated silicon photonic crystals toward terahertz communications," *Journal of Modern Optics*, Vol. 6, No. 16, 1800401, 2018.
7. Yata, M., M. Fujita, T. Nagatsuma, et al., "Diplexer for terahertz-wave integrated circuit using a photonic-crystal slab," *2014 International Topical Meeting on Microwave Photonics (MWP) and the 2014 9th Asia-Pacific Microwave Photonics Conference (APMP)*, 40–43, 2014.
8. Anwar, R. S., L. Mao, H. Ning, et al., "Frequency selective surfaces: A review," *Applied Sciences*, Vol. 8, No. 9, 1689, 2018.
9. Chen, H. T., W. J. Padilla, M. J. Cich, et al., "A metamaterial solid-state terahertz phase modulator," *Nature Photonics*, Vol. 3, No. 3, 148–151, 2009.
10. Li, J., Y. Zhang, J. Li, et al., "Amplitude modulation of anomalously reflected terahertz beams using all-optical active Pancharatnam-Berry coding metasurfaces," *Nanoscale*, Vol. 11, No. 12, 5746–5753, 2019.
11. Grady, N. K., J. E. Heyes, D. R. Chowdhury, et al., "Terahertz metamaterials for linear polarization conversion and anomalous refraction," *Science*, Vol. 340, No. 6138, 1304–1307, 2013.
12. Jung, J., H. Park, J. Park, et al., "Broadband metamaterials and metasurfaces: A review from the perspectives of materials and devices," *Nanophotonics*, Vol. 1, ahead-of-print, 2020.
13. Kim, I. K. and V. V. Varadan, "Electric and magnetic resonances in symmetric pairs of split ring resonators," *Science*, Vol. 106, No. 7, 074504, 2009.
14. Faruk, A. and C. Sabah, "Terahertz metamaterial absorber comprised of H-shaped resonator within split-square ring and its sensory application," *Optik*, Vol. 192, 162976, 2019.
15. Cohen, D. and R. Shavit, "Bi-anisotropic metamaterials effective constitutive parameters extraction using oblique incidence S-parameters method," *IEEE Transactions on Antennas and Propagation*, Vol. 63, No. 5, 2071–2078, 2015.
16. Smith, D. R., S. Schultz, P. Markoš, et al., "Determination of effective permittivity and permeability of metamaterials from reflection and transmission coefficients," *Physical Review B*, Vol. 65, No. 19, 195104, 2002.
17. Chen, J., Y. Dai, L. Yan, et al., "Steady bound electromagnetic eigenstate arises in a homogeneous isotropic linear metamaterial with zero-real-part-of-impedance and nonzero-imaginary-part-of-wave-vector," *Optics Communications*, Vol. 413, 167–171, 2018.
18. Suzuki, T. and H. Asada, "Reflectionless zero refractive index metasurface in the terahertz waveband," *Science*, Vol. 28, No. 15, 21509–21521, 2020.
19. Zhang, J., P. Tang, L. Yu, et al., "Channel measurements and models for 6G: Current status and future outlook," *Frontiers of Information Technology & Electronic Engineering*, Vol. 21, No. 1, 39–61, 2020.
20. Linden, S., C. Enkrich, M. Wegener, et al., "Magnetic response of metamaterials at 100 terahertz," *Science*, Vol. 306, No. 5700, 1351–1353, 2004.
21. Rockstuhl, C., T. Zentgraf, H. Guo, et al., "Resonances of split-ring resonator metamaterials in the near infrared," *Applied Physics B*, Vol. 84, No. 1–2, 219–227, 2006.